Ceramics-Silikáty 68 (3), 353-359 (2024)
www.ceramics-silikaty.cz doi: 10.13168/cs.2024.0034

STRUCTURAL CHARACTERISATIONS AND THERMAL PROPERTIES OF POTASSIUM-ENRICHED MESOPOROUS 45S5 BIOGLASS NANOPARTICLES

#AMMAR Z. ALSHEMARY*, **, ***, ****, *****, ALI ABRA NASER******, S. M. HAIDARY*******, İSMAIL SEÇKIN ÇARDAKLI********

*Nanomaterials Research Center, School of Natural Science, Wenzhou-Kean University, 88 Daxue Road, Ouhai, Wenzhou 325060, Zhejiang Province, China
**Wenzhou Municipal Key Lab for Applied Biomedical and Biopharmaceutical Informatics, Ouhai, Wenzhou 325060, Zhejiang Province, China
***Zhejiang Bioinformatics International Science and Technology Cooperation Center, Ouhai, Wenzhou 325060, Zhejiang Province, China
****Dorothy and George Hennings College of Science, Mathematics and Technology, Kean University, 1000 Morris Ave, Union, NJ 07083, USA
*****Biomedical Engineering Department, College of Engineering and Technologies, Al-Mustaqbal University, 51001, Babylon, Iraq
******Ministry of Education-General Directorate of Misan Education, Misan 62001, Iraq
*******Department of Food Technology, College of Agricultural Engineering Sciences, Salahaddin University, Erbil, Iraq
********Department of Metallurgical and Materials Engineering, Atatürk University, Erzurum, 25240, Turkey

#E-mail: aalshema@kean.edu

Submitted April 11, 2024, accepted May 15, 2024

Keywords: Bioactive glass, Potassium-enriched, Structural characterisation, Thermal properties

This study uses the sol-gel method to explore the structural and thermal properties of synthesised potassium-doped 45S5 bioactive glass (BG) nanoparticles. The X-ray diffraction (XRD) revealed the crystalline phase of $Na_2Ca_4(PO_4)_2SiO_4$ and a shift in diffraction peaks due to the potassium integration, suggesting enhanced crystallinity. Field Emission Scanning Electron Microscopy (FESEM) showed a change in particle morphology with the potassium addition, indicating modified nucleation and growth processes. The thermogravimetric analysis (TGA) demonstrated improved thermal stability in the potassium-doped samples, with reduced weight loss across all temperature ranges. The nitrogen adsorption-desorption isotherm analysis revealed an increase in the surface area from 11.54 $m^2 \cdot g^{-1}$ in the BG to 11.77 $m^2 \cdot g^{-1}$ in the potassium-doped BG and a decrease in the pore volume and average pore size, indicating a significant structural change. These results highlight the potential of potassium-doped BG in biomedical applications, offering enhanced bioactivity and thermal stability.

INTRODUCTION

45S5 Bioactive glass (BG) is a bioceramic that may bind with hard tissues in the host body. This substance, first prepared by Hench, is a quaternary composite comprised of silicon dioxide (SiO_2), calcium oxide (CaO), sodium oxide (Na_2O), and phosphorus pentoxide (P_2O_5) [1, 2]. It is well-known for its high bioactivity and osteoconductive qualities, making it a good candidate for use in bone repair. BG, discovered about four decades ago, has continually enthralled material scientists due to its exceptional bioactivity, which allows osteointegration [3]. The primary way in which this bioactivity is shown is via the development of apatite on the surface of the BG in response to physiological fluids [4]. When exposed to physiological fluids, the BG surface forms apatite, which is the primary way that this bioactivity is proven [5], as coatings for various implants [6], and in the creation of scaffolds [7].

Two main manufacturing methods have been used to produce BG particles. The first technique, called melt-quenching, calls for combining and heating the basic oxides that make up the BG to their melting temperatures inside a platinum crucible. After the mixture reaches a molten state, it is quickly cooled, or "quenched," to produce a glass [8]. This quick cooling procedure keeps the material amorphous, a feature of glass, by preventing the creation of a crystalline structure [9]. However, a significant drawback is the BG particles' limited porosity due to the melt-quenching process. The quick change from a high-temperature liquid to a solid state does not give enough time for a porous structure to

emerge [10]. For many bioactive applications, porosity is essential because it affects the material's surface area and capacity to support biological processes, including vascularisation, nutrient transport, and cell adhesion, all necessary for tissue integration and regeneration [11].

Because it affects the material's surface area and capacity to support biological processes, including cell adhesion, nutrition transport, and vascularisation, crucial for tissue regeneration and integration, porosity is essential for many bioactive applications [12]. These sol-gel-generated BG particles have an increased porosity and surface area [13] and are superior in drug delivery applications. The release profile of medicines may be precisely controlled to promote cellular activity. Due to its versatility, the sol-gel method is very appealing for developing scaffolds in regenerative medicine and other biomedical applications where the material's interaction with the biological environment is critical.

The use of BG is frequently linked to its reduced antibacterial activity and comparatively lower mechanical strength. Several researchers have suggested changing BG's structure by adding metallic and non-metallic oxide dopants to its framework to overcome these restrictions. The glass may have increased angiogenic and antibacterial properties by strategically including such elements. Numerous metal ions, including lithium, silver, bismuth, copper, strontium, niobium, zinc, ferric, and gadolinium, have been incorporated into the BG matrix. Research has shown that these additions enhance the material's bioactive and therapeutic properties, especially in promoting vascular growth and bone formation [14-20].

Potassium is a silvery-white alkali metal well-known for its crucial function in biological systems. It is one of the most prevalent elements on Earth and is essential for many physiological functions, such as controlling nerve messages and muscle contractions in living things [21]. Potassium has garnered interest in biomaterials due to its ability to improve the characteristics of bioactive glasses. Known for its capacity to form bonds with soft tissues and bone, BG may be molecularly altered to customise how it interacts with the human body. Adding potassium ions to the BG's silica network during this doping procedure could significantly change the behaviour of the glass. According to Slimen et al., fluorapatite's structural, mechanical, and thermal characteristics are greatly influenced by the potassium substitution, with the maximum performance noted at a certain substitution amount. This implies that the meticulous management of potassium levels is crucial while developing these materials for particular uses [22].

An intriguing new direction in biomaterial research is the creation of potassium-doped bioactive glass, which promises to produce more specialised and efficient materials for scaffolds for tissue regeneration and medical implants.

EXPERIMENTAL

Tetraethyl orthosilicate ($SiC_8H_{20}O_4$, Merck), commonly abbreviated as TEOS, triethyl phosphate ($C_6H_{15}O_4P$, Merck) or TEP, calcium nitrate tetrahydrate ($Ca(NO_3)_2{\cdot}4H_2O$, Merck), sodium nitrate ($NaNO_3$, Merck), and potassium nitrate (KNO_3, Merck) served as the precursors for the silicon dioxide (SiO_2, Merck), phosphorus pentoxide (P_2O_5), calcium oxide (CaO), sodium oxide (Na_2O), and potassium oxide (K_2O), respectively.

The sol-gel method synthesised BG and BG doped with potassium (K- BG). Using this approach, 2.25 mL of a 1 M nitric acid (HNO_3) solution was first made, and it was then combined with 48.6 mL of water (H_2O). The hydrolysis of the TEOS precursor was started by adding 33.5 mL of TEOS to this acidic solution. For 60 minutes, this combination was allowed to react, guaranteeing complete hydrolysis. Additional reagents were produced independently and mixed for 45 minutes to ensure homogeneity. Among them were 2.9 mL of TEP, 13.52 grams of sodium nitrate, 20.13 grams of calcium nitrate, and potassium nitrate (KNO_3).

These separate ingredients were prepared and then mixed to create a transparent sol. After that, this sol was put in a container and left to stand at room temperature for 5 days without being disturbed to allow for gelation. This is an essential phase because it triggers the construction of a typical gel network structure, which is three-dimensional. The final gel was allowed to age for a day at 70 °C in a sealed container following gelation. This ageing process strengthens the gel's network. To eliminate any last traces of moisture, the aged gel was next dried for 24 hours at 120 °C in an oven. The dried gel was subjected to heat treatment as the last stage of the synthesis to eliminate any last nitrates. To do this, the sample was heated for two hours at 800 °C in a benchtop muffle furnace. By stabilising the BG and La-doped BG's structures, this high-temperature treatment also helps to guarantee that the appropriate chemical composition and characteristics are attained.

The BG and K-BG specimens were thoroughly characterised using a range of analytical methods. The phase composition of the materials was evaluated using X-ray diffraction (XRD, Rigaku Ultima IV), which measured the crystallinity of the samples by methodically scanning from 20° to 80° at 0.03° increments. Fourier transform infrared spectroscopy (FTIR, Bruker IFS66/S) was used to analyse the powders' chemical vibrations and functional groups, giving each molecule a distinct spectral fingerprint. A field emission scanning electron microscope (FESEM, Quanta 400F) with elemental mapping capabilities was used to clarify the morphology and elemental makeup of the samples. The powders were dissolved in ethanol and sonicated for thirty minutes to break up aggregates before drying at room temperature and ready for FESEM imaging.

By tracking mass changes as the temperature was raised from room temperature to 950 °C, the thermogravimetric analysis (TGA, PerkinElmer Pyris 1) assessed the materials' thermal behaviour and provided light on the compositional changes and stability of the samples under heat. Finally, a multipoint BET analysis of the Brunauer, Emmett, and Teller (BET-Multiple point, Quantachrome Corporation – Autosorb 6) technique was used to quantify the textural properties of the powders, including the pore size distribution, total pore volume, and specific surface area. The adsorption characteristics of the powders, which are essential factors for their possible use in various industries, such as tissue engineering and medication administration, are primarily determined by this procedure.

RESULTS AND DISCUSSION

The X-ray diffraction (XRD) spectra in Figure 1 depict the crystallographic patterns of the BG and K-BG, synthesised via the sol-gel technique. It has been well-documented that bioactive glass begins to crystallise when subjected to temperatures exceeding 800 °C. The recorded diffraction patterns correspond to the recognised standard for the crystalline form of $Na_2Ca_2Si_3O_9$, known as combeite (referenced by JCPDS No. 075-1687), resulting in a composite matrix that is predominantly amorphous, but enriched with phosphorus. Distinct and sharp diffraction peaks, particularly prominent at angles of 33.6° and 34.2°, were ascribed to the (024) and (220) crystal planes, respectively. Combeite crystallisation is most abundant at approximately 800 °C, a phenomenon typically associated with the volatilisation of calcium oxide from the composition of the glass matrix [23]. Moreover, the XRD analysis also revealed the presence of a phosphorus-rich, apatite-like crystalline phase, identified as $Na_2Ca_4(PO_4)_2SiO_4$ (referenced by JCPDS No. 032-1053). The intensity of these characteristic peaks increased with the addition of potassium to the BG matrix, suggesting that the K ions were successfully integrated into the structure of the BG. Furthermore, the diffraction peaks shifted to lower two-theta values. This shift is likely to result in the expansion of the lattice parameters [24], which could be attributed to the ionic replacement of Ca ions (with an ionic radius of 0.100 nm) by K ions (with a larger ionic radius of 0.133 nm) [25]. The appearance of sharper peaks and the shift in peaks suggest that potassium ions may have been incorporated into the glass network. This could lead to the formation of new crystalline phases or enhance the growth of existing crystalline structures within the bioactive glass. This integration likely promotes the formation of new crystalline phases within the glass matrix, which may enhance the material's bioactive properties and its potential for application in areas such as bone repair and regenerative medicine.

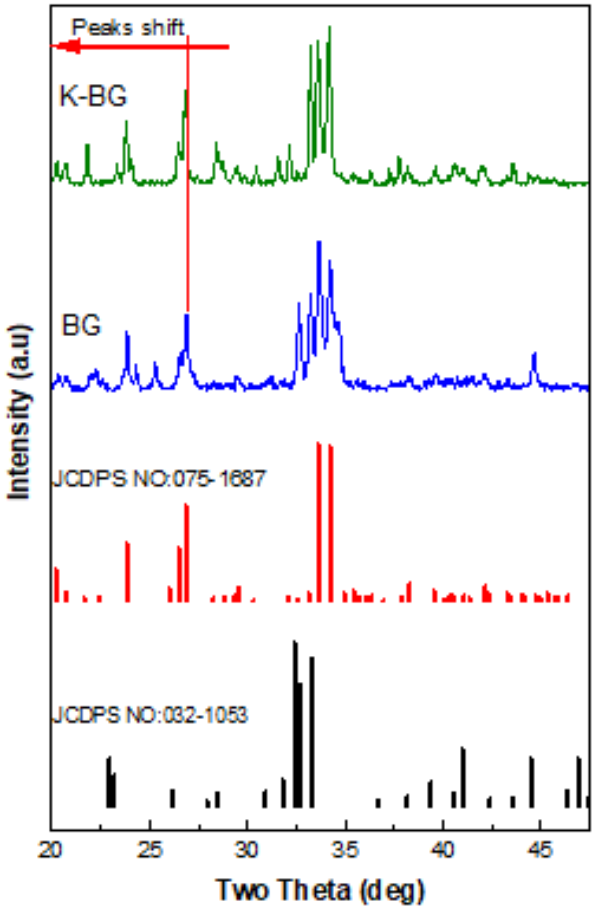

Figure 1. XRD patterns of the BG and K-BG materials.

A diverse range of sizes and shapes can be seen in the FESEM pictures of the BG particles (Figure 2a). The majority of the particles have a coarse surface roughness and an uneven, amorphous form. The particles are between nano and sub-micron in size. The longest dimension of most particles appears to be between 100 and 300 nanometres. Additionally, smaller particle agglomerates combine to create bigger, irregularly shaped clusters. These are common in powders that are handled in ways that result in partial sintering or when high surface energy leads the particles to adhere to one another [26]. Adding potassium shows particles with a substantial shift in the overall texture and potentially the size distribution, but with an erratic morphology (Figure 2b). Compared to earlier times, the particles seem less amorphous and faceted. Some particles even have angular characteristics that could point to the start of crystal development or formation. The particles appear to have a somewhat larger average particle size and a tighter size distribution. The creation of more distinct particle morphologies and a possible rise in the average size are suggested by the faceting and growth into bigger particles, which indicate that the addition of potassium may have impacted the nucleation and growth processes. [24, 27]. This alteration in the morphology may be a sign of several underlying physical or chemical processes,

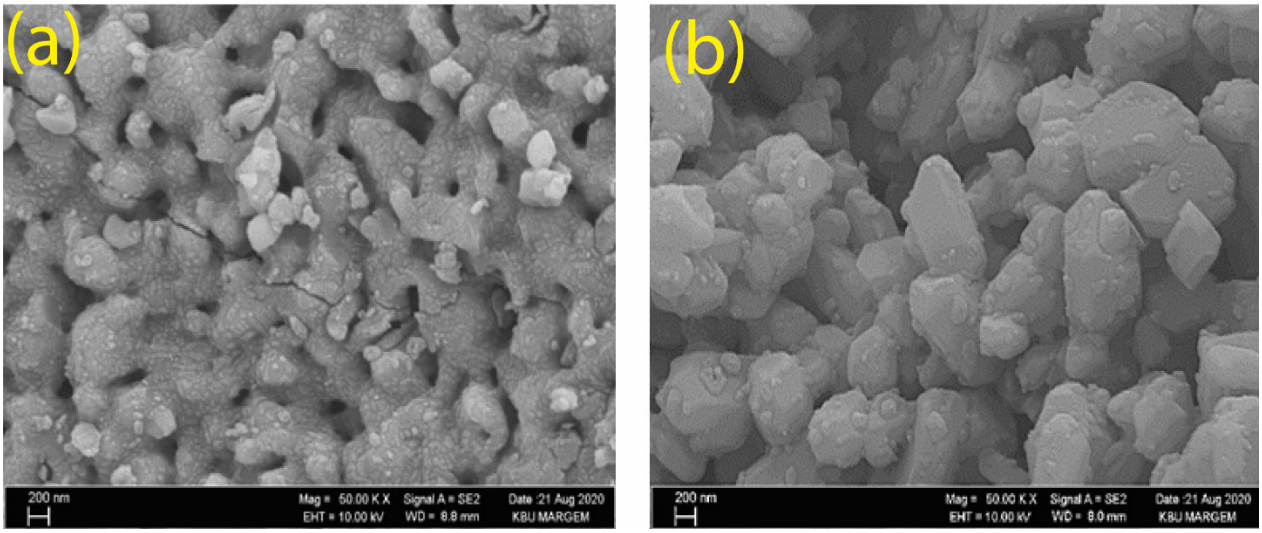

Figure 2. FESEM images of the BG and K-BG materials.

including changed solubility, melting temperatures, or structural changes brought on by adding potassium ions to the glass. These alterations can impact the material's bioactivity, solubility, and interactions with the biological environment.

The FTIR spectra of the BG and K-BG materials are shown in Figure 3. The spectra display discrete, harmonic bands in the 766 to 1175 cm^{-1} range, which can be attributed to the asymmetric stretching of Si-O bonds.

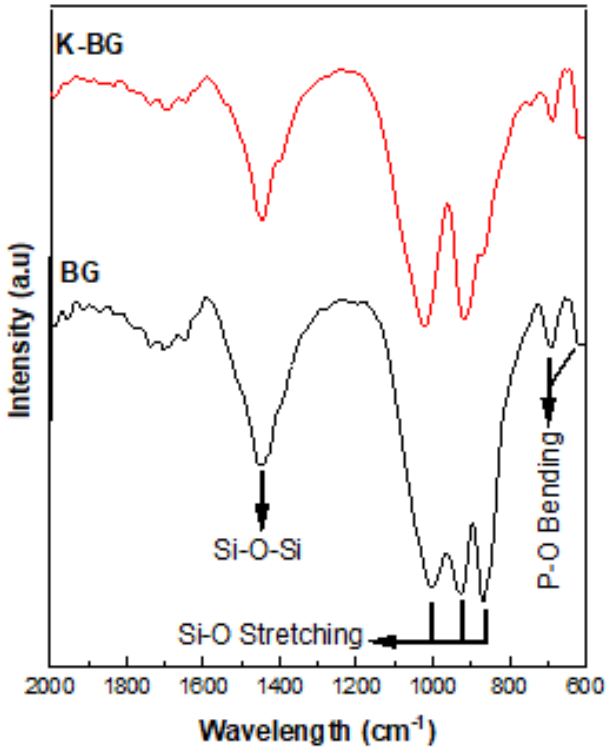

Figure 3. FTIR spectra of the BG and K-BG materials.

The Si-O-Si vibrational mode is probably indicated by the prominent peak that is found at 1443 cm^{-1}. Furthermore, it is possible to link the two different peaks at 611 and 692 cm^{-1} to the bending vibrations of the P-O bonds inside phosphate groups. The absorption band between 611 and 692 cm^{-1}, indicative of the PO_4^{3-} ion's antisymmetric bending, verifies that phosphorus has been incorporated into the glass matrix as an orthophosphate. The spectrum also identifies the O-H symmetric stretching vibration mode, which is visible at around 3613 cm^{-1} and is a distinctive feature in the profile of the silicate glasses. This band is an obvious indicator of these glasses' hygroscopic properties, which means they are more likely to interact with and absorb water molecules. Adding K does not considerably change this specific component of the glass's chemistry, indicating that the BG's basic hygroscopic nature remains unchanged even after potassium doping. This characteristic is important because it suggests that water plays a part in the bioactive behaviour of these glasses and may affect how they respond on the surface when they come into contact with biological fluids [28].

As shown in Figure 4, TGA was used to determine the thermal stability and compositional changes upon heating the BG and K-BG. The TGA thermograms identify three unique temperature periods as the locations of various thermal events: (I) Between 30 °C and 151 °C, the desorption of physically adsorbed water molecules on the material's surface occurs; (II) Between 151 °C and 264 °C, water incorporated into the material's structure evaporates, along with any organic constituents that decompose and volatilise; and (III) Between 264 °C and 714 °C, there is a significant weight loss that is attributed to the breakdown and release of nitrate entities from the glass matrix.

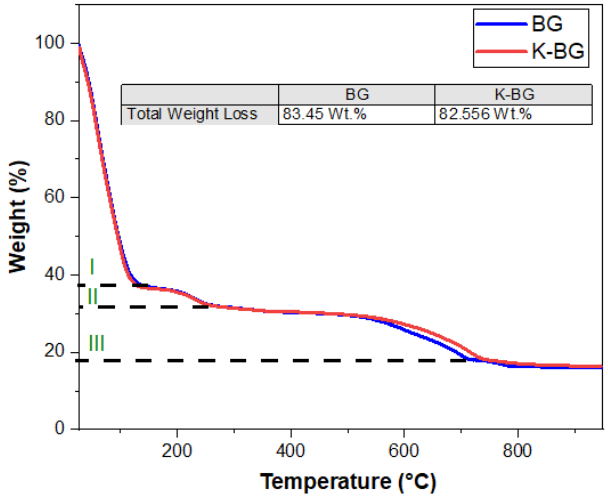

Figure 4. TGA graph of the BG and k-BG materials.

It was shown that adding potassium to the BG framework affected the thermal degradation profile and reduced the weight loss in all the temperature ranges tested. This discovery implies that the K-BG composite could include more crystals with greater thermal stability than the undoped BG [29]. The TGA results shed light on how potassium doping affects the bioactive glass's structural and chemical integrity, which may influence how it behaves in biological and environmental contexts. These results emphasise how crucial the thermal analysis is when determining whether a material is appropriate for a particular application where stability and heat resistance are important considerations.

Figure 5 illustrates the nitrogen adsorption-desorption isotherm approach used to evaluate the textural features of BG and K-BG materials. By analysing the interactions between nitrogen gas and the surface at different pressures, these isotherms offer crucial insights into the pore architecture of materials. Following the international union of pure and applied chemistry (IUPAC) criteria, the isotherms' categorisation as Type IV clearly indicates that the materials are mesoporous, meaning they have pores with widths ranging from 2 to 50 nanometres. Particularly significant is the occurrence of Type H1 hysteresis loops in these isotherms, which support the mesoporosity and imply a homogeneity in the pore size and shape that is frequently linked to materials with distinct cylindrical pores or one-dimensional channel-like structures [28].

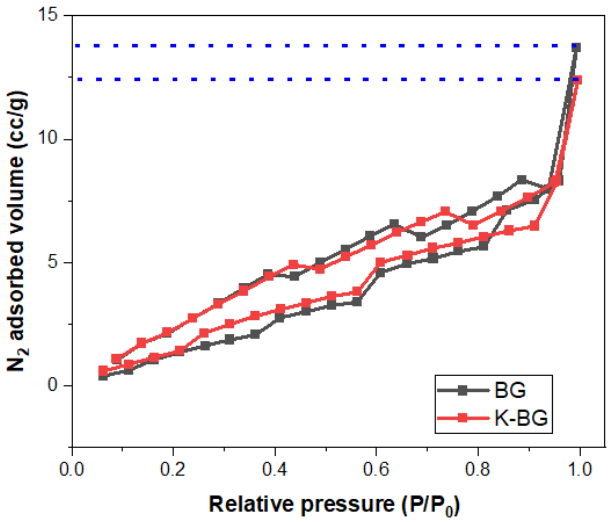

Figure 5. N_2 adsorption–desorption isotherm.

Quantitative measurements of the textural characteristics of the materials were obtained from the analytical data obtained from these isotherms, which were compiled in Table 1. The surface area of the BG increased significantly after doping with potassium, as seen by the swelling of the surface area from a moderate 11.54 $m^2 \cdot g^{-1}$ to a more robust 11.77 $m^2 \cdot g^{-1}$. This improvement suggests that more surfaces are available for possible interactions or reactions. According to pore volume measurements, the pore volume dropped from 0.2491 cc/g in the undoped BG to 0.2267 cc/g in the K-BG, indicating a reduction in the empty spaces inside the material's structure. Furthermore, a considerable reduction in average pore width from 31.35 Å to 22.48 Å indicates a shrinkage of the channels inside the mesoporous structure. When potassium is added, the surface area increases, and the pore volume (and pore width) decreases, indicating a structural change in the BG matrix. This is a sign that the doping process is expanding or developing new pores, either by partially causing the original glass network to dissolve or making it easier for new pore-forming phases to form.

These textural modifications have a wide range of effects. They could fundamentally impact the material's mechanical strength and rate of deterioration. Functionally speaking, a material's efficacy in applications like medication administration can be improved by increasing its surface area. The results, therefore, show that potassium doping modifies the BG's chemical composition and dramatically redesigns its internal architecture. This property may be used to customise the material for specific biological uses.

CONCLUSIONS

This research successfully demonstrates the potential of potassium-doped 45S5 bioactive glass nanoparticles for enhanced biomedical applications. Incorporating potassium ions into the BG matrix significantly modifies its structural and thermal properties. These changes include increased crystallinity, as evidenced by the XRD analysis, and altered morphology with larger, more defined particles, revealed by the FESEM. The TGA results indicated improved thermal stability with reduced

Table 1. Textural parameters obtained by the N_2 adsorption measurement.

	BG	K-BG
Surface Area Data ($m^2 \cdot g^{-1}$**)**		
Multipoint BET	11.54	11.77
BJH Method Cumulative Adsorption Surface Area	14.15	14.64
BJH Method Cumulative Desorption Surface Area	23.11	22.32
DH Method Cumulative Adsorption Surface Area	14.52	14.96
DH Method Cumulative Desorption Surface Area	25.38	24.27
DR Method Micro Pore Area	10.20	10.59
Pore Volume Data (cc/g**)**		
BJH Method Cumulative Adsorption Pore Volume	0.2491	0.2267
BJH Method Cumulative Desorption Pore Volume	0.2868	0.2574
DH Method Cumulative Adsorption Pore Volume	0.2424	0.2207
DH Method Cumulative Desorption Pore Volume	0.2906	0.2603
DR Method Micro Pore Volume	0.03637	0.03774
HK Method Cumulative Pore Volume	0.01532	0.01707
SF Method Cumulative Pore Volume	0.01705	0.01830
Pore Size Data (Å**)**		
BJH Method Adsorption Pore Diameter (Mode)	31.35	22.48
BJH Method Desorption Pore Diameter (Mode)	21.33	21.33
DH Method Adsorption Pore Diameter (Mode)	31.35	22.48
DH Method Desorption Pore Diameter (Mode)	21.33	21.33
DR Method Micro Pore Width	76.77	68.93
DA Method Pore Diameter (Mode)	30.20	28.20
HK Method Pore Width (Mode)	18.52	3.675
SF Method Pore Diameter (Mode)	34.37	4.292

weight loss across the temperature ranges. Additionally, the BET analysis showed increased surface area and decreased pore volume and size, indicating a denser, more compact structure. These findings suggest that potassium-doped BG possesses improved characteristics over traditional BG, making it a promising candidate for tissue engineering and drug delivery applications. The study opens avenues for further exploration of doped bioactive glasses in regenerative medicine.

REFERENCES

1. Meechoowas E., Tungsanguan O., Pamok C., Tapasa K. (2023). Investigation of morphology, structure and bioactivity of bioactive glass. *Materials Today: Proceedings*, In Press. doi: 10.1016/j.matpr.2023.04.643
2. Hench L.L. (1991): Bioceramics: from concept to clinic. *Journal of the American Ceramic Society, 74*, 1487-1510. doi: 10.1111/j.1151-2916.1991.tb07132.x
3. Kargozar S., Kermani F., Mollazadeh Beidokhti S., Hamzehlou S., Verné E., Ferraris S., Baino F. (2019): Functionalization and surface modifications of bioactive glasses (BGs): tailoring of the biological response working on the outermost surface layer. *Materials, 12*, 3696. doi: 10.3390/ma12223696
4. Nguyen A. K., Nelson S. B., Skoog S. A., Jaipan P., Petrochenko P. E., Kaiser A., et al. (2023) : Effect of simulated body fluid formulation on orthopedic device apatite-forming ability assessment. *Journal of Biomedical Materials Research Part B: Applied Biomaterials, 111*, 987-995. doi: 10.1002/jbm.b.35207
5. Jafari N., Habashi M.S., Hashemi A., Shirazi R., Tanideh N., Tamadon A. (2022): Application of bioactive glasses in various dental fields. *Biomaterials Research, 26*, 31. doi: 10.1186/s40824-022-00274-6
6. Hammami I., Gavinho S.R., Jakka S.K., Valente M.A., et al. (2023): Antibacterial Biomaterial Based on Bioglass Modified with Copper for Implants Coating. *Journal of Functional Biomaterials, 14*, 369. doi: 10.3390/jfb14070369
7. Mendoza-Cerezo L., Rodríguez-Rego J.M., Soriano-Carrera A., Marcos-Romero A.C., Macías-García A. (2023): Fabrication and characterisation of bioglass and hydroxyapatite-filled scaffolds. *Journal of the Mechanical Behavior of Biomedical Materials*, 105937. doi: 10.1016/j.jmbbm.2023.105937
8. Islam M.T., Parsons A.J., Nuzulia N.A., Sari Y.W., Ren H., Booth J., Ahmed I. (2023): Process parameter optimisation for manufacturing porous bioactive silicate glass microspheres via flame spheroidisation: The goldilocks effect. *Journal of Non-Crystalline Solids, 614*, 122393. doi: 10.1016/j.jnoncrysol.2023.122393
9. Bhaskar P., Kumar R., Maurya Y., Ravinder R., et al. (2020): Cooling rate effects on the structure of 45S5 bioglass: Insights from experiments and simulations. *Journal of Non-Crystalline Solids, 534*, 119952. doi: 10.1016/j.jnoncrysol.2020.119952
10. Zheng K., Sui B., Ilyas K., Boccaccini A.R. (2021): Porous bioactive glass micro-and nanospheres with controlled

morphology: Developments, properties and emerging biomedical applications. *Materials Horizons, 8,* 300-335. doi: 10.1039/D0MH01498B

11. Ebrahimi M. (2021): Porosity parameters in biomaterial science: definition, impact, and challenges in tissue engineering. *Frontiers of Materials Science, 15*, 352-373. doi: 10.1007/s11706-021-0558-4
12. Du T., Li H., Sant G., Bauchy M. (2018): New insights into the sol–gel condensation of silica by reactive molecular dynamics simulations. *The Journal of Chemical Physics, 148*. doi: 10.1063/1.5027583
13. Kaur G., Pickrell G., Sriranganathan N., Kumar V., Homa D. (2016): Review and the state of the art: sol–gel and melt quenched bioactive glasses for tissue engineering. *Journal of Biomedical Materials Research Part B: Applied Biomaterials, 104*, 1248-1275. doi: 10.1002/jbm.b.33443
14. Cordero H.P., Cid R.C., Dosque M.D., Ibacache R.C., Fluxá P.P. (2021): Li-doped bioglass® 45S5 for potential treatment of prevalent oral diseases. *Journal of Dentistry, 105*, 103575. doi: 10.1016/j.jdent.2020.103575
15. Qian G., Zhang L., Liu X., Wu S., Peng S., Shuai C. (2021): Silver-doped bioglass modified scaffolds: A sustained antibacterial efficacy. *Materials Science and Engineering: C, 129*, 112425. doi: 10.1016/j.msec.2021.112425
16. Wang L., Long N.J., Li L., Lu Y., et al. (2018): Multi-functional bismuth-doped bioglasses: combining bioactivity and photothermal response for bone tumor treatment and tissue repair. *Light: Science & Applications, 7*, 1. doi: 10.1038/s41377-018-0007-z
17. Choe Y.-E., Kim Y.-J., Jeon S.-J., Ahn J.-Y., et al. (2022): Investigating the mechanophysical and biological characteristics of therapeutic dental cement incorporating copper doped bioglass nanoparticles. *Dental Materials, 38* 363-375. doi:10.1016/j.dental.2021.12.019
18. Uskoković V., Abuna G., Ferreira P., Wu V.M., et al. (2021): Synthesis and characterization of nanoparticulate niobium- and zinc-doped bioglass-ceramic/chitosan hybrids for dental applications. *Journal of Sol-Gel Science and Technology, 97*, 245-258. doi: 10.1007/s10971-020-05442-5
19. Zhu D.-Y., Lu B., Yin J.-H., Ke Q.-F., et al. (2019): Gadolinium-doped bioglass scaffolds promote osteogenic differentiation of hBMSC via the Akt/GSK3β pathway and facilitate bone repair in vivo. *International Journal of Nanomedicine, 1085-110*0. doi: 10.2147/IJN.S193576
20. Chiu K.-Y., Chen K.-K., Wang Y.-H., Lin F.-H., Huang J.-Y. (2020): Formability of Fe-doped bioglass scaffold via selective laser sintering. *Ceramics International, 46*, 16510-16517. doi: 10.1016/j.ceramint.2020.03.216
21. Manville R.W. (2019): Potassium-The Essence of Life, *School Science Review, 101*, 57-59.
22. Slimen J.B., Hidouri M., Ghouma M., Salem E.B., Dorozhkin S.V. (2021): Sintering of potassium doped hydroxy-fluorapatite bioceramics. *Coatings, 1*1, 858. doi: 10.3390/coatings11070858
23. Baranowska A., Leśniak M., Kochanowicz M., Żmojda J., Miluski P., Dorosz D. (2020): Crystallization kinetics and structural properties of the 45S5 bioactive glass and glass-ceramic fiber doped with Eu^{3+}. *Materials, 13*, 1281. doi: 10.3390/ma13061281
24. Yokota T., Honda M., Aizawa M. (2017) : Fabrication of potassium-substituted hydroxyapatite ceramics via ultrasonic spray-pyrolysis route. *Phosphorus Research Bulletin, 33*, 35-40. doi: 10.3363/prb.33.35
25. Xie H., Wang Q., Ye Q., Wan C., Li L. (2012): Application of K/Sr co-doped calcium polyphosphate bioceramic as scaffolds for bone substitutes. *Journal of Materials Science: Materials in Medicine, 23,* 1033-1044. doi: 10.1007/s10856-012-4556-z
26. Tsantilis S., Pratsinis S.E. (2004). Soft-and hard-agglomerate aerosols made at high temperatures. *Langmuir, 20*, 5933-5939. doi:10.1021/la036389w
27. Weissmueller N.T., Schiffter H.A., Pollard A.J., Tas A.C. (2014): Molten salt synthesis of potassium-containing hydroxyapatite microparticles used as protein substrate. *Materials Letters, 128*, 421-424. doi: 10.1016/j.matlet.2014.04.154
28. Goh Y.-F., Alshemary A.Z., Akram M., Kadir M.R.A., Hussain R. (2014): In-vitro characterization of antibacterial bioactive glass containing ceria. *Ceramics International, 40,* 729-737. doi: 10.1016/j.ceramint.2013.06.062
29. Kannan S., Ventura J., Ferreira J. (2007) : Synthesis and thermal stability of potassium substituted hydroxyapatites and hydroxyapatite/β-tricalciumphosphate mixtures. *Ceramics International, 33*, 1489-1494. doi: 10.1016/j.ceramint.2006.05.016